PII: S0955-2219(97)00087-3

Kinetics of Weight Changes and Morphological Developments During Oxidation of Pressureless Sintered β-SIALONS

R. Ramesh, P. Byrne, S. Hampshire and M. J. Pomeroy

Materials Research Centre, University of Limerick, Ireland

Abstract

The oxidation behaviour of yttria densified β-sialon materials $(Si_{(6-z)}Al_zO_zN_{(8-z)})$ with z-values of 0·2, 0·5, 1·0, 1·5, 2·0 and 3·0 at 1350°C is reported for times up to 256 h. The sialons can be grouped into two categories with respect to oxidation kinetics and predominant crystalline phases formed in the surface layers. For the z = 0·2 to 1·0 materials, changes in oxidation parabolic rate constant occur after 128 h and yttrium disilicate or cristobalite are the major crystalline oxidation products within the surface layers. For the higher z-value materials, no changes in parabolic oxidation rate are observed and mullite is the predominant phase formed. Examination of cross-sectioned specimens of the z = 0·2 and 3·0 materials indicates changes in morphology consistent with those reported for the surface layers. The kinetics and mechanism of oxidation and morphological development of the oxide scale are discussed in terms of additive diffusion effects. © *1997 Elsevier Science Limited.*

Résumé

Le comportement à l'oxydation de matériaux β-SiAlON $(Si_{(6-z)} Al_z O_z N_{(8-z)})$, densifiés par ajout d'oxyde d'yttrium et ayant des valeurs de z de 0·2 ,0·5, 1·0, 1·5, 2·0 et 3·0, a été suivi à 1350°C pour des temps allant jusqu'à 256 h. Ces matériaux peuvent être groupés en deux catégories suivant les cinétiques d'oxydation et la nature des phases cristallines formées en surface. Pour des valeurs de z comprises entre 0·2 et 1·0, des évolutions de la constante parabolique de la vitesse d'oxydation apparaissent après 128 h de traitement. Les principaux produits d'oxydation à l'intérieur de la couche formée sont le silicate d'yttrium ou la cristobalite. Pour les matériaux ayant des valeurs de z > 1, aucun changement de la constante parabolique d'oxydation n'est observé, et

la mullite est la phase prédominante. L'observation en coupe de SiAlON de z = 0·2 et 3·0 indique des évolutions de morphologie compatibles avec celles observées en surface. Les mécanismes d'oxydation et le développement microstructural de la couche d'oxydes sont traités en terme d'effets de diffusion.

1 Introduction

Silicon nitride-based ceramics are candidate materials for high temperature structural applications because of their excellent high temperature strength. However, for long-term operation their oxidation behaviour is of major importance. It is well known that the oxidation resistance for nitrogen ceramics densified with the aid of sintering additives depends on the residual secondary phases formed at the grain boundaries.[1,2] These intergranular phases give rise to a polyphase scale during oxidation, which in general is not passive and detrimental to oxidation resistance. In the case of β-sialons, the z-value defining the β-sialon phase $(Si_{(6-z)}Al_zO_zN_{(8-z)})$ has a significant effect on the amount and the viscosity of the intergranular phase formed and thereby on the nature of crystalline phases formed in oxide scales during oxidation.[3-6] For example, Schlichting,[5] and Persson and Nygen,[6] have observed that materials with z-values between 1·0 and 2·0 oxidise more rapidly than materials with higher Al-substitution levels. Intervals between the z-values employed in these studies were, however, large and thus no definite effect of z-value can be assessed. Discontinuities in weight gain–time relationships have been observed[7] and these have been related to changes in oxide scale morphology. Clearly, therefore, it is important to follow the chronological development of oxide scale morphology as well as increases in weight gain. Furthermore, most of the studies

Table 1. Compositions, densities and phase assemblage for materials

Code	Y_2O_3	Si_3N_4	AlN	Al_2O_3	% theoretical density	% β sialon	z-value
0·2M	7·00	87·98	0·65	4·37	96	100	0·22
0·5M	7·03	83·33	1·73	7·9	98	100	0·54
1·0M	7·08	75·59	3·53	13·80	98	100	0·85
1·5M	7·13	68·18	5·33	19·66	98	100	1·51
2·0M	7·18	60·17	7·13	25·52	98	100	2·05
3·0M	7·28	44·82	10·70	37·20	100	100	2·70

All compositions are based on 88·9 v/o of relevent sialon — 11·1 v/o Y-sialon glass of composition (in equivalent %) 28 Y;56 Si;16 Al; 80 O;20 N.

conducted to understand the influence of z values on oxidation emphasize the role of transport phenomena in the bulk of the material.[3,4,8] In addition, the references cited have reported the formation of liquid phases during oxidation. However, whether the formation of such liquids is an effect of the oxidation process or its cause has not been rationalised. Recently, Pomeroy and Ramesh[9] have proposed that a solution—precipitation process— is responsible for the development of oxide scales and that the formation of a liquid phase is an integral part of the oxidation process. Transmission Electron Microscopy (TEM) studies of oxide scales formed on silicon nitride ceramics have now provided evidence for this process.[10] The work reported here attempts to more closely define the effect of z-value, additive diffusion effects, liquid formation and surface morphology on oxidation kinetics and mechanism.

2 Experimental Procedure

β-sialons corresponding to nominal z-values of 0·2, 0·5, 1·0, 1·5, 2·0 and 3·0 containing, theoretically, 11 v/o Y-Si-Al-O-N glass (Table 1) were prepared by ball milling Si_3N_4, Y_2O_3, Al_2O_3 and AlN powders for 24 h in isopropanol using sialon milling media. The mixtures were then homogenised for 30 min, dried and sieved to $<212\,\mu m$. They were then cold isostatically pressed into $40 \times 15 \times 15$ mm bars and pressureless- sintered in a powder bed (50 w/o boron nitride + 50 w/o silicon nitride) at 1700°C for 2 h in flowing nitrogen. The fired densities were measured by the Archimedes principle and were compared with theoretical densities derived from the mass fractions and densities of the relevant sialon and Y-Si-Al-O-N glass phases present in the ceramic. The phase assemblages of the fired materials were determined using X-ray diffraction (XRD) and the z-value of the sialon ceramics was estimated using correlations and data published by Ekstrom *et al.*[11] The relevant compositions of the materials employed in this work are given in Table 1 together with theoretical den-

sities achieved, the z-value determined and phase assemblages observed after firing.

The oxidation experiments were carried out in a tube furnace at a temperature of 1350°C, for 1, 16, 32, 64, 128 and 256 h in static air using specimens $(10 \times 10 \times 2$ mm) of each of the compositions, polished to a $1\,\mu m$ finish. After oxidation, the specimens were weighed and the specific weight change evaluated. The phase assemblages of the surface products were determined using XRD while the morphology of the surfaces was examined using Back Scattered Electron Image (BEI) techniques. Energy-dispersive analyses (EDA) for Si, Y and Al were also conducted over large areas $(2·3 \times 1·6$ mm) of the surface layers in order to establish cation contents in equivalent percentages. The values quoted are the mean of three analyses and the range observed was typically 5% of the mean value. Some selected specimens pertaining to 0·2 and 3·0 materials were also sectioned, polished and examined using scanning electron microscopy.

3 Results

3.1 Kinetics of oxidation

For each of the materials tested, straight-line relationships were observed between the square of specific weight gain and time. In the case of the z = 0·2, 0·5 and 1·0 materials, two straight-line relationships were observed. Thus, after time periods of 128 h, there was a distinct decrease in the slope of the curve indicating a marked decrease in oxidation rate. Due to the fact that a 512 and 1024 h oxidation experiment for the 0·2 material showed the continuation of the line between 128 and 256 h data points[12] it is safe to assume that the change in slope observed is a real effect. No such change in slope was observed for the z = 1·5, 2·0 and 3·0 materials. The parabolic rate constants determined on the basis of the measured weight gains are given in Fig. 1 as a function of z-value. It may be observed from this figure that the rate constants for times in excess of 128 h for the z = 0·2, 0·5 and 1·0 materials are typically an order
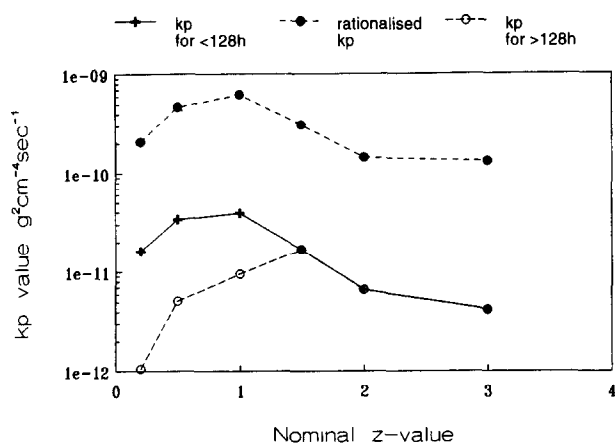
Fig. 1. Parabolic rate constants determined as a function of z-value after oxidation at 1350°C.

of magnitude lower than those observed for times less than 128 h.

In comparing the relative oxidation resistance of β-sialon materials, it is necessary to take into account the fact that as z-values increase the oxygen content of the sialon increases and accordingly the amount of oxygen required for the same extent of oxidation decreases. Because of this, the complete oxidation of one mole of a z = 0·2 sialon requires an oxygen uptake of 78 g, whilst for a z = 3·0 sialon only 50 g of oxygen are required. On this basis, the amount of sialon consumed by oxidation was determined and the corresponding oxidation rate constants were rationalised in terms of z-value. Figure 1 also shows the variation of these rationalised rate constants with z-value. Because of the changes in rate constant for z = 0·2, 0·5 and 1·0 materials, it is difficult to fully compare the oxidation rates with z-value. Accordingly, the total weight gain recorded after 256 h was employed as the most effective method for comparison. Figure 2 shows the variation of extent of weight gain as measured after 256 h and the values of weight gain rationalised with respect to z-value. It is clear from Fig. 2 that the z = 1·0 and 1·5 materials are the least oxidation resistant at a temperature of 1350°C.
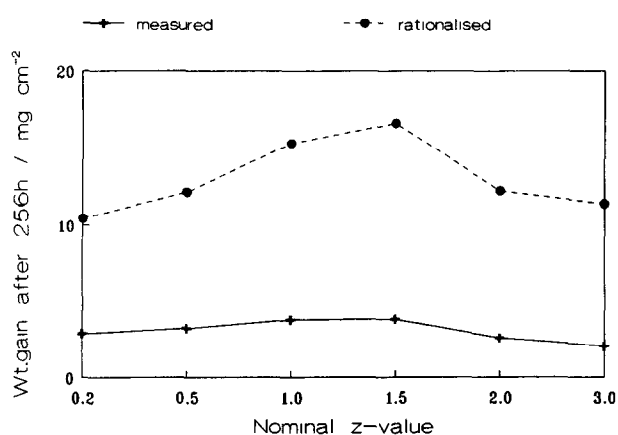

Fig. 2. Variation of weight gain as a function of z-value after 256 h oxidation at 1350°C.

3.2 Phase assemblage of surface products

The phase assemblages observed in the external layers of the oxide scales formed after different time periods are shown in Table 2. From this Table it can be seen that, in general, after 64 h oxidation the phase assemblage becomes effectively constant. The materials may be classified in terms of the predominant phase formed, thus the z = 0·2 material is a silicate former, the z = 0·5 and 1·0 materials are silica formers and the z = 1·0, 2·0 and 3·0 materials are mullite formers. Furthermore, the occurrence of silicon oxynitride in the external layers of the z = 0·2, 0·5, 1·0 and 1·5 materials can be seen after various times of oxidation. The only other nitrogen-containing phases observed were for the z = 3·0 material after 1 h when trace amounts of X-phase (nitrogen mullite) and Y_2SiAlO_5N were detected.

Two further results of note arising from Table 2 relate to the type of yttrium disilicate formed in the surface layers of the z = 0·2, 0·5 and 1·0 materials. It is seen that γ-$Y_2Si_2O_7$ only arises after 64 h oxidation. Furthermore, for the z = 0·2 and 1·0 materials the predominant silicate formed is γ-yttrium disilicate, whilst for the 0·5 material β-yttrium disilicate is the predominant form.

3.3 Surface texture

Typical surface morphologies observed for the z = 0·2, 0·5, 1·0, 1·5, 2·0 and 3·0 materials after 256 h oxidation are shown in Figs 3(a) to (f) respectively. The z = 0·2 material shows a marked level of crystallinity in terms of bright acicular yttrium disilicate crystals in a dark siliceous background. The z = 2·0 and 3·0 materials show similar textures but with needle-like mullite crystals embedded in a Y-Si-Al-containing amorphous phase. In the case of z = 0·5 material yttrium disilicates are seen in the midst of a predominantly silica matrix. The 1·0 and 1·5 materials are typified by the occurrence of needle-like mullite crystals and a grey cristobalite phase located in an amorphous Y-Si-Al-containing phase. It is clear from Figs 3(c) and (d) that the cristobalite content for the z = 1·0 material is greater than that for the z = 1·5 material. This observation is consistent with the XRD data presented in Table 2. The surface textures are reasonably typical of those observed after various times, but most importantly they demonstrate the occurrence of an amorphous Y-containing phase.

3.4 Elemental analysis of surface layers

Table 3 shows cation compositions in equivalent percent derived from the large-area analyses after the various oxidation times and includes the starting composition based on the weights of powders used to fabricate the materials. It may be seen that

Table 2. Phase assemblage observed on surface layers of β-sialons after their oxidation at 1350°C for various durations

Comp.	Phase assemblage					
	1 h	16 h	32 h	64 h	128 h	256 h
0·2M	β-Si$_3$N$_4$ Silica β-Y$_2$Si$_2$O$_7$ SI$_2$N$_2$O^a	Silica β-Y$_2$Si$_2$O$_7$ β-Si$_3$N$_4$	Silica β-Y$_2$Si$_2$O$_7$ β-Si$_3$N$_4$	Silica β-Y$_2$Si$_2$O$_7$ γ-Y$_2$Si$_2$O$_7$	Silica γ-Y$_2$Si$_2$O$_7$^{c} β-Y$_2$Si$_2$O$_7$	γ-Y$_2$Si$_2$O$_7$^{c} Silica β-Y$_2$Si$_2$O$_7$ Si$_2$N$_2$O^a
0·5M	Silica β-sialon β-Y$_2$Si$_2$O$_7$^{a} Mullite^a	Silica β-sialon β-Y$_2$Si$_2$O$_7$ Mullite^a	Silica β-Y$_2$Si$_2$O$_7$ β-sialon Mullite γ-Y$_2$Si$_2$O$_7$^{a}	Silica β-Y$_2$Si$_2$O$_7$ γ-Y$_2$Si$_2$O$_7$ Mullite	Silica β-Y$_2$Si$_2$O$_7$^{b} Mullite γ-Y$_2$Si$_2$O$_7$^{a}	Silica β-Y$_2$Si$_2$O$_7$^{b} Mullite Si$_2$N$_2$O
1·0M	Silica β-sialon Mullite	Silica Mullite β-sialon	Silica Mullite β-sialon Si$_2$N$_2$O β-Y$_2$Si$_2$O$_7$^{a}	Silica Mullite γ-Y$_2$Si$_2$O$_7$^{a}	Silica Mullite γ-Y$_2$Si$_2$O$_7$^{c}	Silica Mullite Si$_2$N$_2$O^a
1·5M	β-sialon Silica Mullite	Mullite Silica β-Sialon	Mullite Silica β-sialon	Mullite Silica Si$_2$N$_2$O^a	Mullite Silica Si$_2$N$_2$O^a	Mullite Silica
2·0M	Silica Mullite β-sialon	Silica Mullite β-sialon	Silica Mullite	Mullite Silica	Mullite Silica	Mullite Silica
3·0M	β-sialon silica Mullite Y$_2$SiAlO5N^a X-phase^a	Mullite Silica β-sialon	Mullite Silica β-siaon	Mullite Silica β-Y$_2$Si$_2$O$_7$	Mullite Silica β-Y$_2$Si$_2$O$_7$	Mullite Silica

$^a\rightarrow$ trace quantity: $^b\rightarrow$ preferred orientation $<110>$: $^c\rightarrow$ preferred orientation $<010>$.

Table 3. Cation compositions of base materials and surface layers (equivalent %)

	Base material	1 h	32 h	64 h	128 h	256 h
z = 0·2						
Y	2·3	24	20	30	35	30
Si	93·8	70	75	67	61	57
Al	3·9	6	6	3	4	13
z = 0·5						
Y	2·4	9	4	18	19	15
Si	90	86	92	77	76	82
Al	7·6	5	4	5	6	3
z = 1·0						
Y	2·4	6	9	10	6	6
Si	83·6	79	65	52	75	73
Al	14	15	26	38	19	22
z = 1·5						
Y	2·5	5	11	8	9	8
Si	76·9	69	47	45	50	46
Al	20·6	26	42	46	41	47
z = 2·0						
Y	2·5	8	6	6	10	7
Si	70·1	59	53	52	50	47
Al	27·4	33	41	42	40	46
z = 3·0						
Y	2·6	11	7	7	8	7
Si	55·7	59	46	53	47	45
Al	41·4	30	47	40	45	48

for each of the materials there is a significant enrichment of yttrium in the surface layers after 1 h. The extent of this enrichment varies with z-value and the enrichment effect is more pro-nounced for the z = 0·2 material. After a period of 64 h, yttrium levels become relatively constant and the yttrium levels observed for the z = 0·2 and 0·5 materials are significantly greater than those
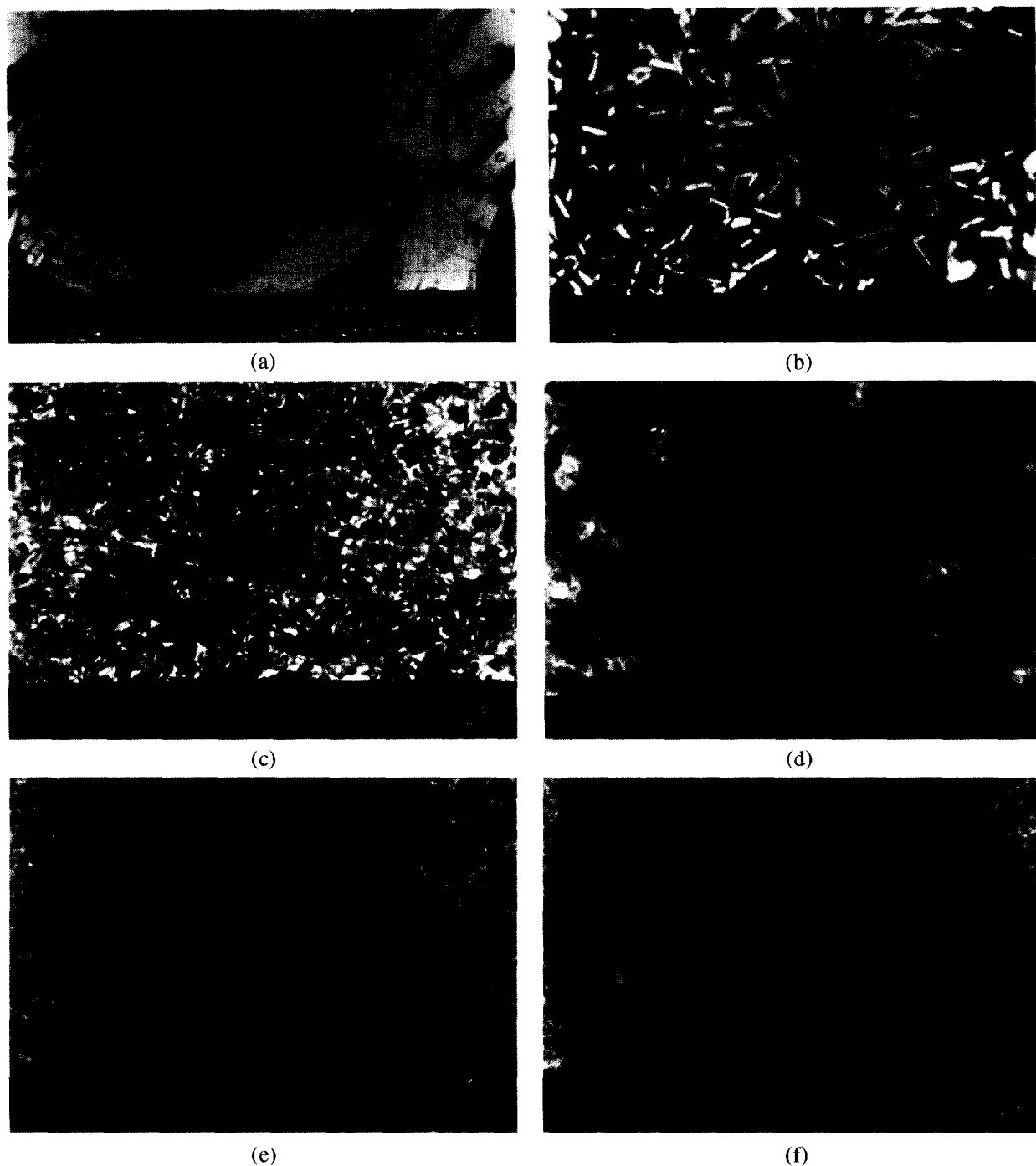
(a)

(b)

(c)

(d)

(e)

(f)

Fig. 3. Surface textures of surface products formed on β-sialon materials after 256 h oxidation at 1350°C (a) $z = 0 \cdot 2$ sialon (b) $z = 0 \cdot 5$ sialon (c) $z = 1 \cdot 0$ sialon (d) $1 \cdot 5$ sialon (e) $2 \cdot 0$ sialon and (f) $3 \cdot 0$ sialon.

observed for the $z = 1 \cdot 0$ to $3 \cdot 0$ materials. In terms of aluminium content, with the exception of $z = 0 \cdot 5$ and $3 \cdot 0$ materials, there is an initial enrichment in the surface layers after 1 h. In the case of the mullite forming $z = 1 \cdot 5$, $2 \cdot 0$ and $3 \cdot 0$ materials, aluminium contents become constant after 32 h oxidation. For the $z = 1 \cdot 0$ material there is a gradual enrichment in aluminium up to 64 h, followed by a significant decrease after 128 h after which the aluminium level is constant.

The overall surface compositions obtained after different time periods have been plotted on the oxide face of the Y-Si-Al-O-N phase diagram in Fig. 4 and the following effects are indicated:

(1) After 1 h, with the exception of the $z = 0 \cdot 2$ and $1 \cdot 5$ materials, the compositions lie close to a line joining the oxide eutectic (melting point 1340°C) and silica ($0 \cdot 5$ and $1 \cdot 0$ materials) or the oxide eutectic and the starting compositions ($2 \cdot 0$ and $3 \cdot 0$ materials).

(2) For times of 32 h and greater the overall surface compositions for the $z = 1 \cdot 5$, $2 \cdot 0$ and $3 \cdot 0$ become relatively constant and lie on a line
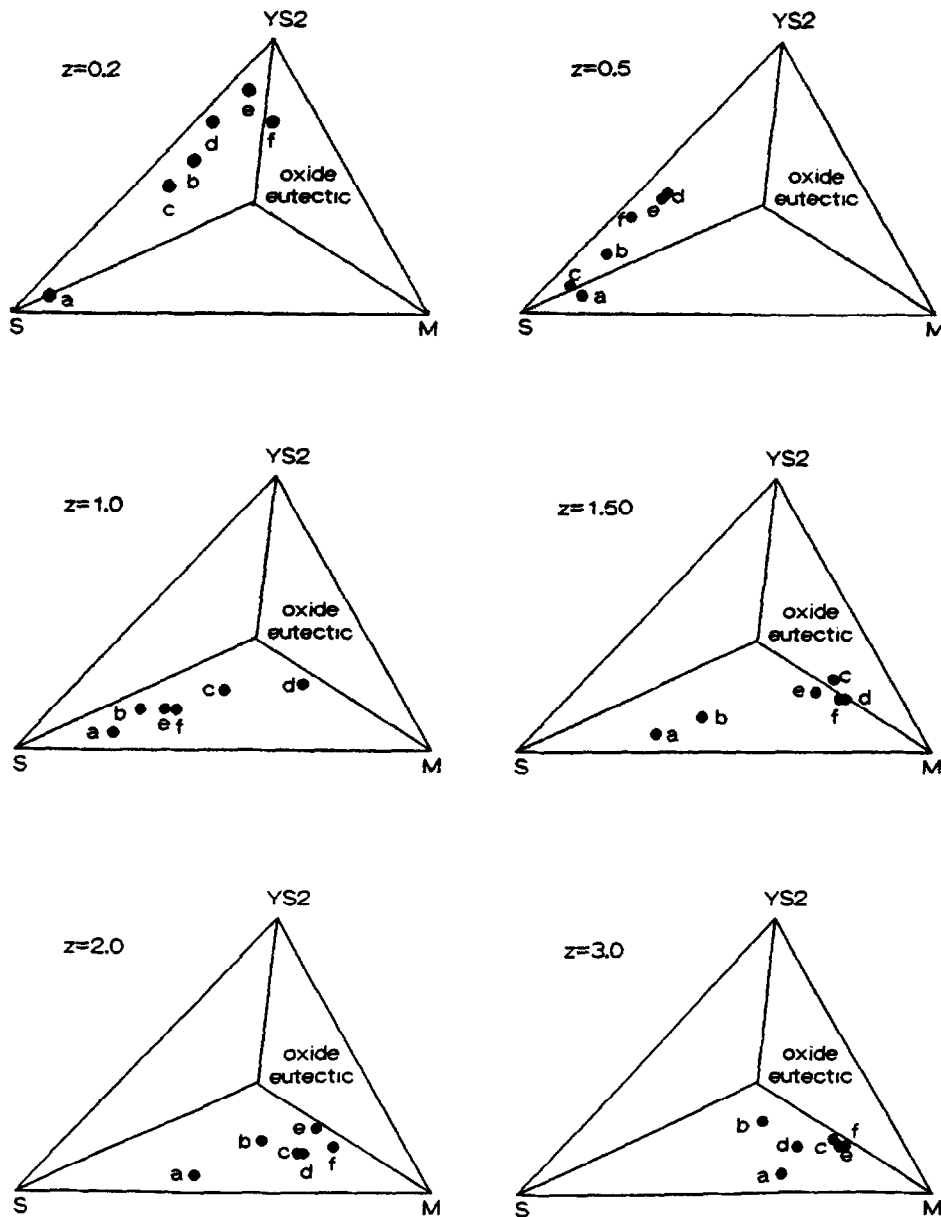
Fig. 4. Large scale surface compositions observed on surfaces of sialon materials after various time periods (a = 0h, b = 1h, c = 32h, d = 64h, e = 128h and f = 256h) S = silica, M = mullite, YS2 = yttrium disilicate (compositions are based on cation (Y, Si and Al) compositions and are expressed in equivalent percentages: the starting compositions are rich in nitrogen and surfaces are also likely to contain nitrogen).

joining mullite and the oxide eutectic, thus confirming the XRD results obtained.

(3) After 32 h the oxide formed on the z = 0·5 material again has a composition close to the line joining the oxide eutectic and silica. For times in excess of 32 h the overall surface composition shifts to a position close to the yttrium disilicate–silica join.

(4) For the z = 0·2 material, the composition gradually shifts toward that of yttrium disilicate and then after 256 h lies close to a line joining yttrium disilicate and the oxide eutectic.

(5) After 1 h oxidation the overall surface composition for the z = 1 0 material lies close to a line joining silica and the oxide eutectic. The

composition then shifts to a point close to the mullite–oxide eutectic line after 32 and 64 h. After 128 and 256 h, the composition returns to a position close to the line joining silica and the oxide eutectic.

The above information demonstrates that for all materials, overall surface compositions lie close to a line joining a crystalline phase and the oxide eutectic at some point during the development of the scale, and that after 128 and 256 h all materials develop surface layers in the scale with compositions which lie close to a line joining yttrium disilicate and the oxide eutectic (z = 0·2), a line joining silica and the oxide eutectic (z = 0·5 and 1·0) or a
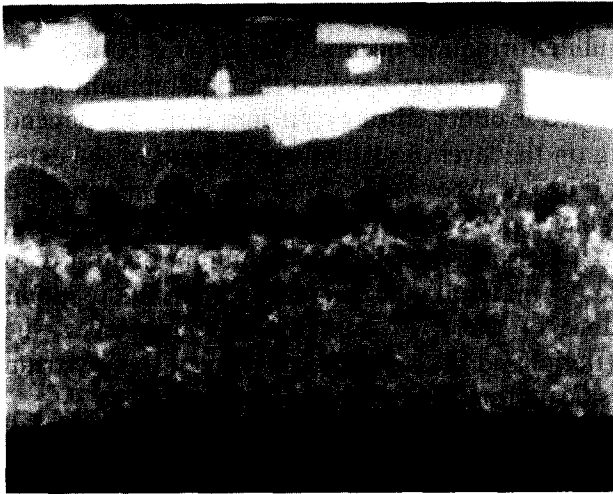
Fig. 5. Cross-sectional back-scattered electron image for z = 0·2 sialon oxidised at 1350°C for 128 h.
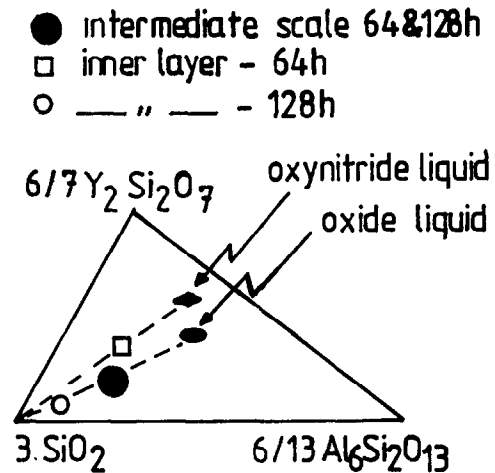

Fig. 7. Cation compositions obtained across oxide layers of z = 0·2 sialon formed after 64 and 128 h oxidation at 1350°C superimposed on part of oxide face of Y-Si-Al-O-N system.

line joining mullite and the oxide liquid (z = 1·5, 2·0 and 3·0).

3.5 Cross-sectional analysis

Figures 5 and 6 show typical cross-sectional back scattered electron images obtained after 128 h oxidation for z = 0·2 and 3·0 materials respectively. It can be seen from Fig. 5 that for z = 0·2 material the morphology comprises an external layer of yttrium disilicate crystals and an yttrium-rich layer adjacent to the underlying bulk ceramic. Examination of the intermediate layer revealed rich levels of silicon and low levels of aluminium and yttrium. The cation compositions obtained from a few energy-dispersive analyses conducted across the oxide layers on the z = 0·2 material are superimposed on part of the oxide face of the Y-Si-Al-O-N Janecke prism in Fig. 7. It is seen from the figure that the compositions of the oxide layers are located close to a line joining silica and the liquid

composition. In the case of the specimens oxidised for 64 h the composition of the yttrium-rich layer adjacent to the underlying ceramic lies on the silca–liquid join but closer to the liquid composition. In contrast, for specimens oxidised for 128 h (and also for 256 h) the composition of the yttrium-rich layer adjacent to the ceramic was located close to the yttrium disilicate–silica join (see Fig. 7).

The z = 3·0 material shows the presence of needle-like mullite crystals in the external layers of the oxide scale (Fig. 6). A high level of porosity can also be seen in the region of the oxide–sialon interface resulting from the evolution of nitrogen during oxidation. Energy-dispersive analysis conducted across the oxide layer indicates an enrichment of yttrium and aluminium in the exterior scale regions while in the region close to the oxide–sialon interface there appears to be an enrichment in aluminium coupled with a depletion in silicon (Fig. 8).
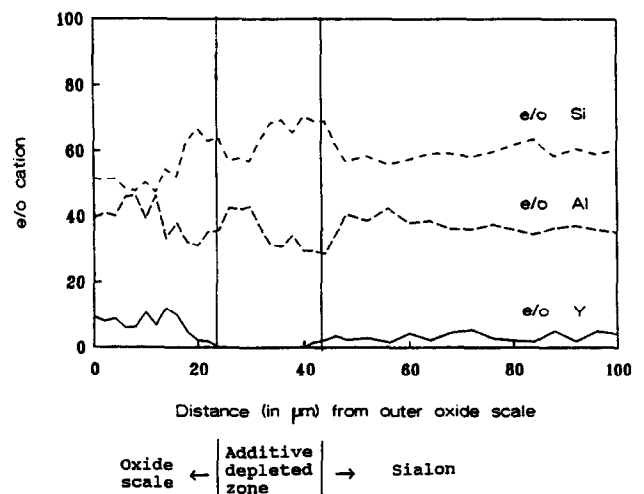

Fig. 6. Cross-sectional back-scattered electron image for z = 3·0 sialon oxidised at 1350°C for 128 h.

Fig. 8. Concentration profiles for silicon, aluminium and yttrium across sialon scale interface (128 h oxidised z = 3·0 sialon).

4 Discussion of Results

From the data presented in Fig. 1 it is clear that comparison of the oxidation resistance of sialons in terms of parabolic rate constants is not possible because of the fact that changes in these constants occur with time. This underlines the necessity for testing sialon materials for long ($>$ 128 h) time periods in order to accurately assess oxidation behaviour. The most valuable information obtained from the evaluation of rate constants was the fact that for the β-sialons with $z = 0.2$, 0.5 and 1.0 changes in rate constant occurred, whilst for the $z = 1.5$, 2.0 and 3.0 materials, no changes in rate constant were observed. The most accurate way of comparing the oxidation resistance of the sialons tested is clear from the information given in Fig. 2. The ranking order of the materials, however, differs depending on whether 'as-measured' or 'rationalised' data are employed in the comparison. Thus, for 'as-measured' data, the ranking order in terms of decreasing oxidation resistance is $3.0 >$ $2.0 > 0.2 > 0.5 > 1.0 > 1.5$ whilst the order when 'rationalised' data are employed is $0.2 > 3.0 > 0.5$ $> 2.0 > 1.0 > 1.5$. This clearly shows that the rationalisation of weight gain data in the manner described above is of major importance. From the results obtained in this work it can be concluded that the most oxidation-resistant materials are the end members of the series ($z = 0.2$ and 3.0). There is no doubt that the materials with the poorest oxidation resistance are the β-sialons with $z = 1.0$ and 1.5.

The above information relating to the long-term oxidation of β-sialons with $z = 0.2$, 0.5 and 1.0 shows that there is an order of magnitude decrease in oxidation rate after 128 h exposure. Furthermore, it is seen that the overall composition of the yttrium-enriched layers present at the ceramic–oxide interface lies closer to a liquid composition at 1350°C after 64 h oxidation than after 128 h oxidation (Fig. 4). These two observations can be rationalised if the rate of oxidation depends on the volume of the liquid formed at the sialon–oxide interface, since after 128 h the lower volume of liquid gives rise to significantly lower rates of solution of the sialon grains. If this mechanism of oxidation is accepted, then the rates of oxidation should be dependent on the volume and viscosity of liquid formed during oxidation. Greater liquid volumes will result in greater extents of silicon nitride/sialon solution and lower viscosities will enable the dissolution products to be transported away from the liquid–nitride interface more rapidly.

With respect to the predominant phase formed in the exterior surface layers it is seen that there is a critical z-value which must be exceeded before mullite formation occurs. This value is between 1.0 and 1.5. For lower z-values the predominant phase formed is either silica or yttrium disilicate depending on the level of yttrium-enrichment in the external layers (see Table 3). Close examination of Table 3 shows that the surface layers of the 0.2 and 1.0 materials are richer in aluminium than those of the 0.5 material and this may explain the predominance of the β-ytttrium disilicate for the $z = 0.5$ material and the preferred stability of the γ-yttrium disilicate for the $z = 0.2$ and 1.0 materials.

The occurrence of nitrogen-containing phases within the exterior layers of the materials (Table 2 eg. Si_2N_2O and Y_2SiAlO_5N) confirms that the scales formed during oxidation contain small levels of nitrogen. Furthermore the Y_2SiAlO_5N phase only arises on devitrification of Y-Si-Al-O-N glasses at temperatures less than 1150°C.[13] Such a reaction is likely to occur via a solution precipitation reaction which would enable a preferred growth mechanism to operate. These observations, in conjunction with the surface textures observed and overall surface compositions of the oxidised materials strongly indicate the presence of an oxynitride liquid phase at the surface during oxidation. The lowest-melting oxynitride liquid in this system has been reported as 1330°C[14] which is close to that of the lowest oxide eutectic temperature (1340°C) and thus liquid phase formation could most certainly occur at the temperature employed in this work.

Whilst the results reported here and those reported elsewhere in the literature[3,4,8] indicate that the diffusion of additive cations (Y and Al in the present case) is the rate-controlling step during oxidation at temperatures of the order of 1350°C, the exact reason for this is not fully appreciated. However, the above observations enable a fuller understanding if it is argued that the diffusion of additive and cation impurities into the surface scale results in a scale composition which is liquid at the oxidation temperature. Further diffusion of cations results in increases in liquid content and lowering of the viscosity of the liquid formed. If liquid phase formation is the effect of additive cation diffusion then the oxidation mechanism must be enabled by liquid phase formation, and since the sintering of these ceramics involves the solution of α-silicon nitride followed by a precipitation of β-silicon nitride or β-sialons, it seems plausible that oxidation can also be facilitated by a solution–precipitation mechanism.

In order to elucidate this further, a cold isostatically pressed $z = 0.2$ specimen was fired in a boron nitride/silicon nitride powder bed for 96 h in flowing nitrogen at 1350°C, that is, at the temperature

used for the oxidation experiments. The resulting material had undergone significant densification as the initial green density of 62% of theoretical had increased to nearly 90% and there was significant reaction to form approximately 65% β-sialon. The results from this experiment clearly show that at a temperature of 1350°C silicon nitride can undergo a solution–precipitation reaction. Accordingly, it is reasonable to infer that the oxidation of the β-sialon materials results from a solution of the β-sialon grains into liquid regions of the oxide scale, followed by the decomposition of the nitrogen-saturated liquid to produce nitrogen bubbles and a residual oxide glass containing small levels of nitrogen, as indicated by the presence of nitrogen-containing phases in the surface layers of the oxidised ceramics.

As stated earlier, Backhaus-Ricault and Gogotsi[10] have recently provided direct TEM evidence of silicon nitride grain solution during the oxidation of a hot-pressed silicon nitride densified with yttria and alumina additives. In addition, Fordham *et al.*[15] have provided graphic hot-stage micrographs of the surface of an oxidising silicon nitride material which clearly indicate rapid nitrogen release through a violently agitated liquid oxidation product. Such rates of nitrogen release would not be expected to arise if the silicon nitride was first oxidised to silica via the reaction of silicon nitride with oxygen. These findings endorse the postulate that oxidation is facilitated by the solution of sialon grains by aluminosilicate liquids.

5 Conclusions

(1) The most oxidation resistant β-sialons at a temperature of 1350°C are the end members of the series with $z = 0.2$ and 3.0 and the least oxidation-resistant β-sialons are the $z = 1.0$ and 1.5 materials.

(2) The morphological development of oxide scales can be understood in terms of differences between various cation ratios present in the oxide scale layers and those required for liquid phase formation.

(3) Differences in oxidation rates are due to differences in oxidation scale liquid volumes and viscosities.

(4) The kinetics and mechanism of oxidation of silicon nitride ceramics involves the solution of silicon nitride/sialon grains by liquids formed due to cation diffusion effects. Rates and extents of liquid phase formation are dependent on the diffusion of additive cation from within the bulk ceramic to the oxide scale.

References

1. Singhal, S. C., Oxidation of silicon nitride and related materials. In *Nitrogen Ceramics*, ed. F. L. Riley. Noordhoff, Leiden, 1977, pp. 607–626.
2. Clarke, D. R. and Lange, F. F., Oxidation of silicon nitride alloys: relation to phase equilibrium in the system Si_3N_4-SiO_2-MgO. *J. Am. Ceram. Soc.*, 1980, **63**(9-10), 586–593.
3. Lewis, M. H. and Barnard, P., Oxidation mechanisms in Si-Al-O-N ceramics. *J. Mat. Sci.*, 1980, **15**, 443–448.
4. Pomeroy, M. J. and Hampshire, S., Oxidation processes in a high substitution β-sialon. *Materials Chemistry & Physics*, 1985, **13**, 437–448.
5. Schlichting, J., Oxidation and hot corrosion behaviour of Si_3N_4 and sialon. In *Nitrogen Ceramics*, ed. F. L. Riley. Noordhoff, Leiden, 1977, pp. 627–634.
6. Persson, J. and Nygren, M., Oxidation studies of β-sialons. In *Proceedings of the 11th Riso International Symposium on Metallurgy and Materials Science*, ed. J. J. Bentzen, J. B. Bilde-Sorensen, N. Christiansen, A. Horsewell and B. Ralph. Riso National Laboratory, Roskilde, 1990, pp. 451–457.
7. Andrews, P. and Riley, F. L., The microstructure and composition of oxide films formed during high temperature oxidation of sintered silicon nitride. *J. Euro. Ceram. Soc.*, 1989, **5**, 245–256.
8. Themelin, L., Desmaison-Brut, M., Billy, M. and Crampon, J., Post Densification behaviour of pressureless sintered silicon nitride materials: relationship between properties and microstructure. *Ceramics International*, 1992, **18**, 119–130.
9. Pomeroy M. J. and Ramesh, R., Understanding the morphological development of oxidation products formed on β-sialon materials with different z-values. In *Microscopy of Oxidation-2*, ed. S. B. Newcomb and M. J. Bennett. Institute of Materials Publ., London, 1993, pp. 566–575.
10. Backhaus-Ricoult, M. and Gogotsi, Yu. G., Identification of oxidation mechanisms in silicon nitride ceramics by transmission electron microscopy studies of oxide scales. *J. Mater. Res.*, 1995, **10**(9), 1–16.
11. Ekstrom, T., Kall, P. O., Nygren, M. and Olsson, P. O., Dense single-phase β'-sialon ceramics by encapsulated hot isostatic pressing. *J. Mater. Sci.*, 1989, **24**, 1853–1861.
12. Pomeroy, M. J., Ramesh, R and Hampshire, S., Morphological development of surface scales during long term oxidation of a low Al-substituted β'-sialon. *Key Engineering Materials*, 1994, **89–91**, 283–288.
13. Thompson, D. P., New grain boundary phases for nitrogen ceramics. *Mat. Res. Soc. Symp. Proc.*, 1993, **287**, 79–92.
14. Hohnke and Tien,. T. Y., Solid–liquid reactions in part of the system Si, Al, Y/N,O. In *Nitrogen Ceramics*, ed. F. L. Riley. Martin Nijhoff, The Hague, 1983, pp. 101–110.
15. Fordham R. J., Norton J. F., Canetoli S. and Coste J. F., In situ studies of the surface changes occurring during high temperature oxidation of silicon nitride. In *Microscopy of Oxidation-2*, ed. S. B. Newcomb and M. J. Bennett. Institute of Materials Publ. London, 1993, pp. 545–554.